Adapting Unsigned Signals Between Triaxial Antennas For Use In Magnetic Induction Localization

Francesco Bernardini, Javier Garcia, Conlan C. Taylor, Julien Leclerc and Aaron T. Becker
Department of Electrical and Computer Engineering
University of Houston, Houston, Texas 77204-4005
Email: {fbernardini,jgarciagonzalez,ctaylor16,jleclerc,atbecker}@uh.edu

Abstract—Magnetic induction localization is an inverse problem that determines the relative position and orientation (pose) between transmitting and receiving coils by analyzing the received signals. Related work has established methods to resolve the localization into two candidate poses. However, these methods require having signed signals, or periodic signals whose starting point is unambiguously determined with respect to an absolute reference (the transmitted signal). For distributed systems, the signal signs are difficult to resolve. This paper presents a method to extract partial information about the signs from unsigned signals. The method is tested in a hardware experiment.

Index Terms-Localization, Magnetic Induction, Robotics

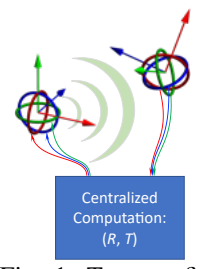
I. Introduction

Magnetic induction (MI) has found use across a broad range of fields. Inductive coils are employed for subsurface sensing and in geological surveying. Recently, some robotics applications have begun employing MI for navigation and sensing. MI has also been proposed for localizing distributions of wireless sensor networks for data collection and monitoring.

We are particularly interested in applying this technology to underwater localization systems, to enable collision avoidance between underwater remotely operated vehicles (ROVs) and autonomous underwater vehicles (AUVs). The most relevant methods toward this end are those which can perform localization in general 3-D environments without prior knowledge of other actors in the workspace. This type of problem manifests as a *distributed* computation scheme, where a transmitted signal and received signal are processed on separate systems, as opposed to a *centralized* one, where computation occurs on the same system (Fig 1).

Furthermore, additional constraints ought to be considered in these environments. Excessively large or heavy devices may prove impractical for maneuvering and buoyancy. Power consumption may be limited to on-board power supplies for an extended duration of time without the aid of external computers and charging. And due to the difficulty of communication,

This research is supported by Texas Commission on Environmental Quality through an award to the Subsea Systems Institute, and by the National Science Foundation under Grant No. [IIS-2130793] and [IIS-1849303]. This project was paid for in part with federal funding from the Department of the Treasury through the State of Texas under the Resources and Ecosystems Sustainability, Tourist Opportunities, and Revived Economies of the Gulf Coast States Act of 2012 (RESTORE Act). The content, statements, findings, opinions, conclusions, and recommendations are those of the author(s) and do not necessarily reflect the views of the State of Texas or the Treasury.



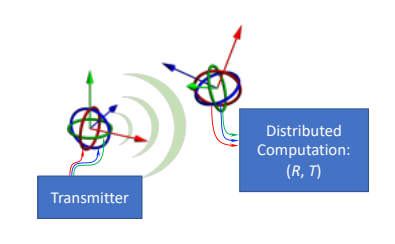


Fig. 1: Two configurations of transmitter and receiver pairs in a centralized computation scheme (left) and a distributed computation scheme (right).

reduction of the system's dependence on extraneous sensors is desirable.

II. RELATED WORK

In previous work we used induced voltages to estimate the distance between two triaxial antennas. A particle filter was then applied, with the velocity information of the actors carrying the antennas, to iteratively select the best estimates [1]. However, the particle filter was applied offline to recreate an already traversed path. Velocity information was just assumed to be shared between the agents. Moreover, several iterations of the filter were needed before useful estimates could be produced. We are interested in alternate methods that may offer ways to mitigate or eliminate such drawbacks entirely.

Some methods used to optimize power transfer in wireless charging utilize phased arrays or grids of coils to determine the relative position of a target device by monitoring changes in the phase difference [2] or mutual inductances [3], [4] of the sensing elements. Qui et al. adopt a similar approach by using an array of sensing elements within an inductive transmitting coil for localizing buried metallic objects [5]. While useful for their intended purposes, the nature of such designs would make the MI sensors highly directional, and therefore unsuitable for omnidirectional sensing.

Similar to our prior work, a number of authors [6]–[9] have tested MI localization methods using triaxial coil antennas as transmitters (Tx) and receivers (Rx), which provide omnidirectional sensing patterns better suited to 3-D localization problems. That said, some features of these methods make implementing them in our application infeasible. Huang and Zheng's proposed method [9] requires the use of more than one triaxial antenna. Tan and Sun present a method for localizing

sensor network nodes in magnetically-noisy environments [7]. In addition to requiring two triaxial antennas for noise identification, this method is intended solely for determining the position of the nodes, not their orientation. Abrudan et al. offer both position and orientation estimation using only a single antenna, but rely on an additional IMU sensor to provide the orientation data [8].

Furthermore, many electromagnetic tracking algorithms require some means of relating the phases of the nine signals between the three collocated Tx coils and three collocated Rx coils [6], [10]–[13]. One way to determine this is to directly compare the received signals with those sent by the Tx. However, since we wish to use these tracking algorithms for localization and collision avoidance of untethered robots – hence, in a distributed computation scheme and not a centralized one – Rx units are assumed to have little to no prior knowledge of the Tx signal properties.

III. LOCALIZATION USING RELATIVE SIGNS

MI occurs in the reactive near field of an EM source. Assuming the source is pointlike, the extension of the near field can be approximated [14] as a spherical region whose radius depends on frequency f and the speed of light in the medium c_m :

$$R_{nf} = \frac{c_m}{2\pi f} \ . \tag{1}$$

In air at a frequency of $50\,\mathrm{kHz},$ such as in our case, this radius is approximately $950\,\mathrm{m}.$

Underlying the localization methods we are considering is the assumption that the received signals contain information about the relative Tx position. This is a geometrical fact, linked to how the lines of a magnetic field concatenate with the surface of a coil to generate a magnetic flux. By Faraday's law, the derivative of such flux generates a voltage difference at the ends of the coil.

We refer to a *signed* signal as a waveform for which the slope of the time derivative can be unambiguously determined at its origin (when a Tx coil is actuated). Therefore, if the signal is sampled at an arbitrary time and no further information about its origin (i.e. its phase with respect to the Tx which produced it) is available, we cannot conclude anything about its sign, and therefore we regard it as *unsigned*. If we receive multiple generated signals that share the same origin and features, it is possible to define the notion of a *relative sign*. In the simplest case of two sinusoids with the same frequency and coinciding zeroes (see Fig. 3), they are assigned a relative sign of +1 if the sinusoids are in phase and -1 if they are in antiphase.

The method of Kim et al. [10] (KSP algorithm) solves for an unknown rotation matrix R and position offset p from the Tx antenna to the Rx antenna. Assuming that the Tx and Rx coils are identical and that the coils in each antenna are mutually orthogonal, we can say

$$S = R^{\top} \cdot \frac{A\mu}{4\pi \|p\|^3} \left(3\hat{p}\hat{p}^{\top} - I \right), \tag{2}$$

where μ is the permeability, A is a constant related to the magnetic moments of the Tx and the characteristics of the Rx, and S is the 3×3 amplitude matrix of the received magnetic flux, assumed to be a sinusoidal signal of constant frequency. Then,

$$S = [\mathbf{s}_x, \mathbf{s}_y, \mathbf{s}_z] = \begin{bmatrix} s_{xx} & s_{xy} & s_{xz} \\ s_{yx} & s_{yy} & s_{yz} \\ s_{zx} & s_{zy} & s_{zz} \end{bmatrix}, \tag{3}$$

where s_{ij} , for $i, j \in \{x, y, z\}$, corresponds to the magnetic flux in coil i due to the signal generated by coil j. The wavelengths of the signals considered in the present paper $(\sim km)$, compared to the dimensions of the Tx and Rx and their relative distance (fractions of m), are large enough to justify both the MI assumption and the quasi-static approximation, which are implicit in Eq. 2. Specifically, Eq. 2 assumes no phase shifts among the 9 sinusoidal signals, and the S matrix captures them at an instant when each of them is either at a crest or a trough. The least squares solution provides one R, but two antipodal p. Using unsigned signal amplitudes, each of the 9 elements in S can be either positive or negative. Given |S|, there are $2^9 = 512$ ways to reconstruct S. This generates 512 rotations and 1024 potential positions. Half of the candidate R values will not be valid rotation matrices, but we are still left with 256 candidate rotation matrices and 512 candidate positions, for a total of 512 candidate poses.

Our goal is to reduce the number of candidate poses by analyzing the relationship between received unsigned signals, extracting their relative signs, and reducing the number of ways to reconstruct S.

In general, the received signals are detected by onboard instrumentation as a voltage or current. If we assume to pick up the signal once all transients have expired and the steady state sinusoidal signal has been established, the collectable information is then an unsigned signal amplitude, which we can use to populate the following matrix U:

$$U = \begin{bmatrix} u_{xx} & u_{xy} & u_{xz} \\ u_{yx} & u_{yy} & u_{yz} \\ u_{zx} & u_{zy} & u_{zz} \end{bmatrix}. \tag{4}$$

As in (3), each column corresponds to the Rx response to a signal generated by one of the coils of the Tx, but in this case $u_{ij} \geq 0$ by construction. |U| is related to |S| by a scaling constant ξ , which encompasses the effects of the circuitry attached to the Rx coils. For simplicity, we assume all the circuits have similar parameters.

Lacking the Tx connection, the only observable quantity at the Rx's end are the amplitudes and the relative phases between the three Rx coils generated by the same source signal. The latter are determined by two concurrent factors:

- Position and orientation: Reversing a coil's orientation reverses the flux's sign, and subsequently imparts a 180° phase shift on the detected waveform. On the other hand, position affects the intensity of the received flux.
- *The network characteristics*: Each of the three Rx coils can be modeled as an RLC series resonant circuit (Fig. 2),

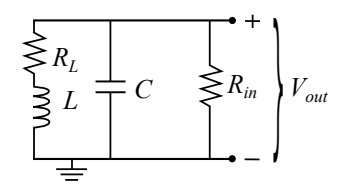


Fig. 2: The circuit model for the antennas used in our setup, including the input resistance R_{in} of the measuring device. The voltage is measured at the edges of the capacitor.

where L is the coil inductance, R_L is its parasitic resistance, C is the capacitance, and R_{in} is the input resistance of the measuring apparatus. The resonant frequency is $\omega_c = 1/\sqrt{LC}$.

It can be shown that the circuit imposes an overall phase shift on the measured signal:

$$\phi = \arctan\left(\frac{\omega L}{R_L}\right) - \arctan\left(\frac{\omega\left(CR_L + \frac{L}{R_{in}}\right)}{1 + \frac{R_L}{R_{in}} - \omega^2 LC}\right). \tag{5}$$

With this in mind, along with the unsigned amplitudes matrix U, we can introduce the matrix Φ of the relative phases and the matrix Σ of the relative signs

$$\Phi = \begin{bmatrix} \phi_{yx,x} & \phi_{yx,y} & \phi_{yx,z} \\ \phi_{zx,x} & \phi_{zx,y} & \phi_{zx,z} \\ \phi_{zy,x} & \phi_{zy,y} & \phi_{zy,z} \end{bmatrix}, \Sigma = \begin{bmatrix} \sigma_{yx,x} & \sigma_{yx,y} & \sigma_{yx,z} \\ \sigma_{zx,x} & \sigma_{zx,y} & \sigma_{zx,z} \\ \sigma_{zy,x} & \sigma_{zy,y} & \sigma_{zy,z} \end{bmatrix}.$$
(6)

where, $\phi_{ij,k} = \phi_j - \phi_i$ and $\sigma_{ij,k}$ is the relative sign of the channels i and j, when k coil is transmitting. Our purpose is to define a suitable algorithm to derive Σ from Φ .

A. Ideal Case

If the Rx coils are assumed to be identical, and if the Tx signal oscillates with frequency ω_c , then each Rx coil will experience the same phase shifts resulting from circuit induction effects. In this case, a scenario like that shown in Fig. 3 will occur, where the three signals oscillate either in phase or in antiphase. In other words, the relative signs of the signals are only driven by the position of the Rx antenna. In terms of the relative phase shifts, the constraint

$$\phi_{yx} - \phi_{zx} + \phi_{zy} = 2k\pi, \ (k \in \mathbb{Z}) \tag{7}$$

allows only four phase combinations, each corresponding to two sets of absolute signs:

$$\{\phi_{yx}, \phi_{zx}, \phi_{zy}\} = \begin{cases} \{0^{\circ}, & 0^{\circ}, & 0^{\circ}\} & \to & (\pm \pm \pm)^{T}, \\ \{0^{\circ}, & 180^{\circ}, 180^{\circ}\} & \to & (\pm \pm \mp)^{T}, \\ \{180^{\circ}, & 180^{\circ}, & 0^{\circ}\} & \to & (\pm \mp \mp)^{T}, \\ \{180^{\circ}, & 0^{\circ}, & 180^{\circ}\} & \to & (\pm \mp \pm)^{T}. \end{cases}$$
(8)

B. Practical Considerations

In the real world, the electrical characteristics of each coil (R, L, C) have some level of tolerance. These deviations manifest in non-identical phase shifts between channels, so even though the constraint (7) will still hold, the phase shifts among the channels become $\phi_{ij} = \{\tilde{\phi}_{ij}, \tilde{\phi}_{ij} + 180^\circ\}$. The

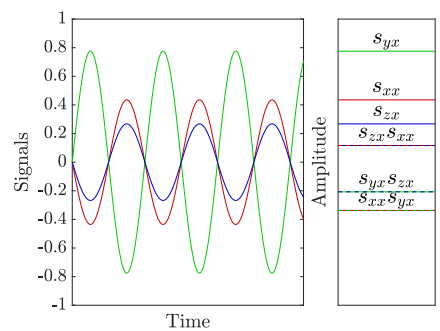


Fig. 3: Example of received signals from coil x. Although from the plot it is not possible to infer the absolute sign of the signals, we can still obtain information about their relative signs. In the picture s_{xx} and s_{zx} are in phase while both are in antiphase with s_{yx} .

phases ϕ_{ij} are properties of the network that can be predicted theoretically and verified experimentally.

C. Localization Algorithm

The phase between two sinusoids with an otherwise identical period T = 1/f is given by

$$\int_{t_0}^{t_0+T} \sin(2\pi f t + \phi_1) \sin(2\pi f t + \phi_2) dt = \frac{1}{2f} \cos(\phi_1 - \phi_2).$$
 (9)

This integral is positive if $\phi_{21} \equiv (\phi_1 - \phi_2) \in (-90^\circ, 90^\circ)$, zero for $\phi_0 = \pm 90^\circ$, and negative in every other case. An analog to digital converter measuring the induced signals samples every T_s seconds, assumed for simplicity a submultiple of $T = NT_s$, $N \in \mathbb{N}$. For the actual computation of the phase shift, we may use the time series

$$c_{ij,k} = \sum_{m=1}^{N} u_{ik}[t_0 + t_m] \cdot u_{jk}[t_0 + t_m], \ \{i, j, k\} \in [x, y, z], \ (10)$$

where $u_{ik}[t_n]$ is the t_n -th element of the sequence of samples received from coil i when coil k transmits, t_0 is an arbitrary starting time, and $t_m = mT_s$ (the time series extends over one period). In the ideal case, even with some degree of measurement noise, the relative phase between any two channels is expected to lie in a close neighborhood around 0° or 180° . This means that in order to assess if two signals are in phase or antiphase, it is enough to declare their phase shift to be smaller or larger than 90° , respectively. The sign properties of the time series – inherited from (9) – suggest that, given nine sequences $u_{ij}[t_n]$ of received sampled signals, the matrix of relative signs (6) can be populated

$$\Sigma = \begin{bmatrix} \operatorname{sgn}(c_{yx,x}) & \operatorname{sgn}(c_{yx,y}) & \operatorname{sgn}(c_{yx,z}) \\ \operatorname{sgn}(c_{zx,x}) & \operatorname{sgn}(c_{zx,y}) & \operatorname{sgn}(c_{zx,z}) \\ \operatorname{sgn}(c_{zy,x}) & \operatorname{sgn}(c_{zy,y}) & \operatorname{sgn}(c_{zy,z}) \end{bmatrix},$$
(11)

with the distinction that every time a $c_{ij,k} = 0$, two matrices Σ_{\pm} are generated with a ± 1 in the (i,j) element. According to (8), each column of Σ corresponds to two possible absolute sign choices. Then, only eight possible candidate matrices are left to determine the pose of the Rx.

As a final remark, this approach assumes an ideal system where the network is perfectly matched, so that all the signals from the Rx can be assumed to be in phase or antiphase. In other terms, we pivot a $\pm 90^{\circ}$ window around 0° assigning +1 if the measured phase shift lies therein, or -1 otherwise. This makes $\{0^{\circ},0^{\circ},0^{\circ}\}$ the privileged reference combination for the algorithm.

As discussed in Sec. III-B, real systems have the propensity to experience additional phase shifts $\tilde{\phi}_{ij}$ due to unavoidable tolerances in the circuit. The ultimate effect of these phase shifts is an unintended offset of the pivot points of the two $\pm 90^\circ$ windows, which alters the results of (11). Careful modeling allows to us predict the values of the phase shifts by means of (5), but to validate such predictions experimentally may require indirect methods. In Sec. IV, we present a procedure to measure the phase shifts of our antenna system to account for these non-ideal effects.

IV. EXPERIMENTS AND RESULTS

A forward application of the KSP algorithm allows us to generate a matrix S of signed amplitudes corresponding to a given position and orientation of the Rx with respect to the Tx. For simplicity we assumed A = 1, which amounts to generating just the position dependence of a dipolar field, up to a known constant $\mu/4\pi$, in units of magnetic flux. From such a matrix it is possible to extract an unsigned amplitude matrix U and a matrix of relative signs Σ , as in (4) and (6). These matrices can be directly compared with the outcome of amplitude and phase measurements, and manipulated via the algorithm described in Sec. III-C. Ideally, the matrices of the predicted and measured amplitudes are related by ξ parameter in (2). In practice, coils are not perfectly identical, so we expect the ξ parameter to be best described by some kind of distribution. For what concerns the relative signs, on the other hand, we expect the signs predicted by the KSP method to coincide with those obtained applying our algorithm to the measured phases. The algorithm might fail if the phase measurement is noisy, or if the pivot points ϕ_{ij} are not properly set. The metric we selected to assess the effectiveness of the sign algorithm is the rate of success in the prediction of the elements of the matrix Σ of (6).

Finally, the KSP algorithm is based on the magnetic dipole approximation. Consequentially, it loses accuracy when Tx and Rx are in close proximity. The first set of measurements, described in Sec. IV-A, aims to estimate the range of this close-proximity zone, and to determine the phase shifts $\tilde{\phi}_{ij}$ at different octants in the space surrounding the Tx. The second set of measurements, described in Sec. IV-B, focuses on the scaling constant and the sign prediction success rate. The following experimental setup is presented in Fig. 4:

 The Tx a) and Rx b) were realized using two cube coil emitters from Premo (PN 3DCC28-A-0039J), mounted on dedicated supports for easy positioning and stability. The nominal values of the inductances and their DC resistances were found:

$$[L_x, L_y, L_z] = [380, 375, 365] \pm 1 \,\mu\text{H},$$
 (12)

$$[R_x, R_y, R_z] = [1.7, 1.6, 1.8] \pm 0.1 \Omega.$$
 (13)

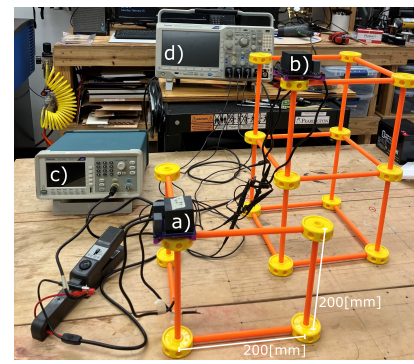


Fig. 4: Experimental setup for the measurements.

The capacitors chosen to realize the Rx RLC circuit models were measured:

$$[C_x, C_y, C_z]^{(rec)} = [27.05, 27.36, 27.26] \pm 0.01 \,\text{nF}.$$
(14)

- Each coil of the Tx was powered by a Tektronix AFG1022 function generator c), imparting a 50 kHz sinusoidal current. Once again, based on Eq. (1), this granted us a near field sphere of 950 m radius, more than sufficient for our measurements. The coils were turned on sequentially, one at a time.
- Currents, voltages and phases were measured with a Tektronix MDO3024 oscilloscope d), and the related data collected along with the corresponding transmitting coil.

Quadrants were labeled according to the following convention: $\{+++\}$ denote the quadrant where x, y and z coordinates of the Rx are all positive, $\{---\}$ when they are all negative, and similarly for all other combinations. We define *opposite pairs* of quadrants whose signs are inverted. For example, $\{+-+\}$ and $\{-+-\}$ form an opposite pair.

A. Experimentally determining coil phase shifts

The first part of the experiment set out to determine the true phase shifts $\tilde{\phi}_{ij}$ of the physical network. Substituting the measured circuit component values into (5), the following absolute phase shifts for each channel were obtained,

$$[\tilde{\phi}_x^{(th)}, \tilde{\phi}_y^{(th)}, \tilde{\phi}_z^{(th)}] = [114 \pm 3^{\circ}, 137 \pm 9^{\circ}, 48 \pm 6^{\circ}], \quad (15)$$

which in turn give rise to the following relative theoretical phase shifts:

$$\tilde{\phi}_{yx}^{(th)} \equiv \tilde{\phi}_x - \tilde{\phi}_y = -23 \pm 12^{\circ},
\tilde{\phi}_{zx}^{(th)} \equiv \tilde{\phi}_x - \tilde{\phi}_z = 66 \pm 9^{\circ},
\tilde{\phi}_{zy}^{(th)} \equiv \tilde{\phi}_y - \tilde{\phi}_z = 89 \pm 15^{\circ}.$$
(16)

These phase shifts represent the theoretical offset for the relative sign algorithm, meaning that the $\pm 90^\circ$ windows will pivot on $-23^\circ/157^\circ$ for $\tilde{\phi}_{yx}$, on $-114^\circ/66^\circ$ for $\tilde{\phi}_{zx}$, and on $-91^\circ/89^\circ$ for $\tilde{\phi}_{zy}$ instead of $0^\circ/180^\circ$. As the phase shifts must respect the general identity

$$\tilde{\phi}_{ux}^{(th)} - \tilde{\phi}_{zx}^{(th)} + \tilde{\phi}_{zy}^{(th)} = 0^{\circ}, \tag{17}$$

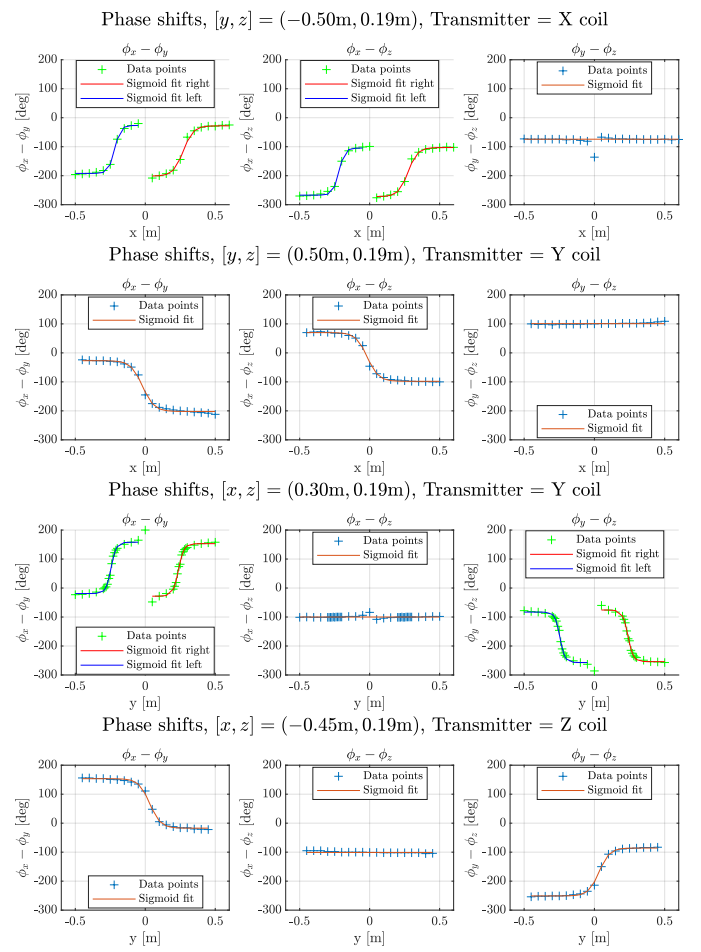


Fig. 5: Phase plots with one coil transmitting, as the Rx moves in a single axis. Depending on the transmitting coil, and sufficiently far from the transmitter, specific combinations of phase shifts correspond to different quadrants.

only the following four combinations are possible:

$$\left\{ \tilde{\phi}_{yx}^{(th)}, \tilde{\phi}_{zx}^{(th)}, \tilde{\phi}_{zy}^{(th)} \right\} = \begin{cases}
-23^{\circ}, & 66^{\circ}, & 89^{\circ} \\
-23^{\circ}, & -114^{\circ}, & -91^{\circ} \\
157^{\circ}, & 66^{\circ}, & -91^{\circ} \\
157^{\circ}, & -114^{\circ}, & 89^{\circ}
\end{cases} .$$
(18)

In order to experimentally determine the phase shifts, a certain number of relative phase measurements were conducted in the axis-symmetric configuration around the Tx in the $\{+++\}$, $\{+-+\}$, $\{-++\}$ and $\{--+\}$ quadrants.

The Rx was translated along straight trajectories in the x or y direction, and the phase shift was recorded every $0.05\,\mathrm{m}$. The measurement resolution was refined to every $0.01\,\mathrm{m}$ where the phase profile appeared to vary more rapidly. Overall, the behavior of the phase shift was well-approximated by either a sigmoid curve or a flat line. A representative collection of these characteristics is displayed in Fig. 5. The phase exhibits nonlinear behavior within a sphere of approximately $0.2\,\mathrm{m}$ around the Tx, and across specific planes that cross the Tx which depend on the orientation of the Rx. For example, in the axis-aligned configuration, the xy, yz and zx planes of the

Tx. Far from the Tx, the phases appeared to settle down to specific, repeatable pairs of values:

$$\tilde{\phi}_{yx}^{(exp)} = \{ -26 \pm 5^{\circ}, 161 \pm 6^{\circ} \},
\tilde{\phi}_{zx}^{(exp)} = \{ -101 \pm 6^{\circ}, 79 \pm 8^{\circ} \},
\tilde{\phi}_{zy}^{(exp)} = \{ -78 \pm 7^{\circ}, 99 \pm 9^{\circ} \}.$$
(19)

These values always occurred in specific combinations

$$\left\{ \tilde{\phi}_{yx}^{(exp)}, \tilde{\phi}_{zx}^{(exp)}, \tilde{\phi}_{zy}^{(exp)} \right\} = \left\{ \begin{array}{l} \left\{ -26^{\circ}, 79^{\circ}, 99^{\circ} \right\} \\ \left\{ -26^{\circ}, -101^{\circ}, -78^{\circ} \right\} \\ \left\{ 161^{\circ}, 79^{\circ}, -78^{\circ} \right\} \\ \left\{ 161^{\circ}, -101^{\circ}, 99^{\circ} \right\} \end{array} \right\}, (20)$$

which, within the experimental error, were compatible with those of (18) and respected the general identity

$$\tilde{\phi}_{yx}^{(exp)} - \tilde{\phi}_{zx}^{(exp)} + \tilde{\phi}_{zy}^{(exp)} = 0^{\circ}. \tag{21}$$

For example, whenever the Rx was found in the quadrant $\{-++\}$ and the Y coil was transmitting, the phase shifts were $\{-26^\circ, 79^\circ, 99^\circ\}$, and whenever the Rx was found in the quadrant $\{+-+\}$ and the X coil was transmitting, the phase shifts were $\{-26^\circ, -101^\circ, -78^\circ\}$. Similarly, the $\{+++\}$ quadrant can be associated with the phase shifts $\{161^\circ, 79^\circ, -78^\circ\}$ when X or Y are transmitting, and $\{161^\circ, -101^\circ, 99^\circ\}$ when Z is transmitting. This result is equivalent to Table II of [12] and Table I of [11], but transposed to the case of nonzero phase shifts. In particular, it suggests that the combination corresponding to $\{+++\}$ in the ideal case, namely $\{0^\circ, 0^\circ, 0^\circ\}$ when X is transmitting, becomes $\{161^\circ, -101^\circ, 99^\circ\}$ in the real case. This claim is confirmed in Sec. IV-C.

B. Signal measurements

The second set of experiments were aimed at determining the scaling constant A from (2). The Tx antenna was placed at the center of the test bench, while the Rx antenna was positioned at 20 different points in the eight quadrants around the Tx, outside of the breakdown region determined in Sec. IV-A. Two sets of measurements were performed, one with the Rx and the Tx in an axis-aligned configuration, and the other with the Rx rotated by a yaw angle $\psi=45^{\circ}$, for a total of 40 poses.

For each point, labeled by its coordinates [x,y,z] and the orientation of the Rx, the U and Φ matrices were populated by recording peak to peak amplitudes and phase shifts between pairs of channels. By taking the elementwise ratio of the absolute value of the matrix generated by the KSP algorithm with the matrix of measured amplitudes, we obtained a set of numbers that are either zero or positive. The zeros were discarded, as no measurement can ever be less than the noise threshold. The remaining, strictly positive subset was successfully matched with a log-normal distribution (Fig. 6), confirming the validity of Eq. 2 in this context. The parameters of the log-normal distributions in the axis-aligned (a) and $\psi=45^{\circ}$ (b) cases are

$$(\mu^{(a)}, \sigma^{(a)}) = (2.47, 0.57); \quad \text{Mo}^{(a)} = 8.56 \text{Wb/V}, (\mu^{(b)}, \sigma^{(b)}) = (2.41, 0.51); \quad \text{Mo}^{(b)} = 8.59 \text{Wb/V},$$
 (22)

where Mo $\equiv e^{\mu - \sigma^2}$ is the mode of the distributions.

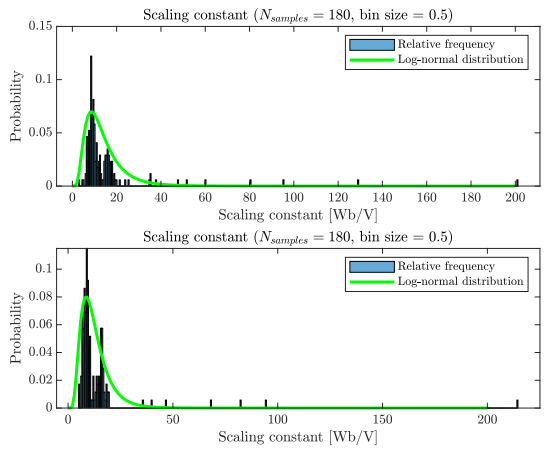


Fig. 6: Scaling constant in axis-aligned and $\psi=45^{\circ}$ configuration. The modes are $\mathrm{Mo}^{(axp)}=8.56\mathrm{Wb/V}$ and $\mathrm{Mo}^{(\psi=45)}=8.59\mathrm{Wb/V}$.

C. Sign prediction success rate

To extend the algorithm to the non-ideal case, we need to identify which of the combinations in (18) maps to $\{0^{\circ}, 0^{\circ}, 0^{\circ}\}$ to provide the new privileged reference set of phase offsets for the algorithm. Feeding the algorithm with different combinations will produce different matrices, so for each pose of Rx we simply compared element-wise the theoretical sign matrix $\Sigma^{(th)}$ with the five matrices $\Sigma_{j}^{(exp)}, j=1,...,5$ obtained using the four combinations in (18) and $\{0^{\circ}, 0^{\circ}, 0^{\circ}\}$. The results of the comparison are summarized in Table I and show a remarkable success of the {161°, -101°, 99°} combination, which independently confirms our claim of Sec. IV-A purely on geometrical considerations. The inaccuracies in relative sign prediction can be ascribed to cases of very low signal strength from one of the Rx coils (therefore difficult reconstruction of the phase shifts involving that channel), or phase shifts very close to the edge of the algorithm's tolerance window.

V. CONCLUSIONS AND FUTURE WORK

This work presented an alternate method related to the MI localization problem based on a distributed computation scheme, which removes the requirement of a direct connection between the Tx and the Rx by exploiting the relationship between the signals at the Rx end only. Furthermore, a thorough analysis of the behavior of the phase shifts between the channels of the Rx antenna has been performed, allowing us to extend the ideal algorithm to a real scenario with arbitrary phase shifts. Within the experimental error, the predicted phase shifts are compatible with the measured values. As the phase shifts depend on the electrical parameters of the system, these results could also be considered as an indirect method to validate the circuit model used. The scaling constant for this specific setup has been determined by fitting the data with a log-normal distribution, showing a definite trend that validates the theoretical expectation. However, the relative signs approach can only decrease the number of pose candidates to 16, versus the 2 of the signed signals method, which suggests a need to explore additional approaches to complement these

results. Further extensions of these ideas might involve using regularities among pairwise *row* data to eliminate candidate localization solutions, identifying individual scaling constants for the nine couplings among Tx and Rx coils, and exploring the behavior of phase with changes in frequency to investigate the properties of a multi-frequency transmission scheme. Finally, additional measurements of the phase shifts can provide better estimates of the phase shifts, thus improving the success rate of the sign prediction.

TABLE I SUCCESS RATES FOR THE PHASE SHIFT CONFIGURATIONS

| | Axis-symmetric | | | $\psi = 45$ | | |
|------------------|----------------|-------|---------|-------------|-------|---------|
| Phase Shifts [°] | Right | Wrong | Success | Right | Wrong | Success |
| $\{0, 0, 0\}$ | 26 | 140 | 16% | 22 | 146 | 13% |
| {161, 79,-78} | 53 | 113 | 32% | | 111 | 34% |
| {161,-101, 99} | 159 | 7 | 96% | 165 | 3 | 98% |
| { -26, 79, 99} | 61 | 105 | | | | |
| { -26,-101,-78} | 59 | 107 | 36% | 58 | 110 | 35% |

REFERENCES

- [1] J. Garcia, S. Soto, A. Sultana, and A. T. Becker, "Localization using a particle filter and magnetic induction transmissions: Theory and experiments in air," in 2020 IEEE Texas Symposium on Wireless and Microwave Circuits and Systems (WMCS), 2020, pp. 1–6.
- [2] V. Ranganathan, B. H. Waters, and J. R. Smith, "Localization of receivers using phased-array wireless power transfer systems," in 2015 IEEE Wireless Power Transfer Conference (WPTC), 2015, pp. 1–4.
- [3] J. Al Sinayyid, H. Takhedmit, P. Poulichet, M. Grzeskowiak, A. Diet, and G. Lissorgues, "A reconfigurable coil grid for receiver localization in wireless power transfer and magnetic field steering," *IEEE Journal of Radio Frequency Identification*, vol. 5, no. 2, pp. 128–138, 2021.
- [4] F. Wen, X. Chu, Q. Li, F. Jing, W. Zhao, and Z. Chu, "Receiver localization and power stabilization for wireless power transfer system," in 2020 IEEE International Conference on Applied Superconductivity and Electromagnetic Devices (ASEMD), 2020, pp. 1–2.
- [5] Y. Qiu, S. Zhang, S. Chen, and C. Luo, "UXO localization procedures applied to potable TEM sensor," in 2019 IEEE 4th Advanced Information Technology, Electronic and Automation Control Conference (IAEAC), 2019, pp. 2239–2242.
- [6] A. Sheinker, B. Ginzburg, N. Salomonski, L. Frumkis, and B.-Z. Kaplan, "Localization in 3-d using beacons of low frequency magnetic field," *IEEE transactions on instrumentation and measurement*, vol. 62, no. 12, pp. 3194–3201, 2013.
- [7] X. Tan and Z. Sun, "Environment-aware indoor localization using magnetic induction," in 2015 IEEE Global Communications Conference (GLOBECOM), 2015, pp. 1–6.
- [8] T. E. Abrudan, Z. Xiao, A. Markham, and N. Trigoni, "Distortion rejecting magneto-inductive three-dimensional localization (MagLoc)," *IEEE Journal on Selected Areas in Communications*, vol. 33, no. 11, pp. 2404–2417, 2015.
- [9] H. Huang and Y. R. Zheng, "Node localization in 3-d by magnetic-induction communications in wireless sensor networks," in OCEANS 2017 Anchorage, 2017, pp. 1–6.
- [10] W. Kim, J. Song, and F. C. Park, "Closed-form position and orientation estimation for a three-axis electromagnetic tracking system," *IEEE Transactions on Industrial Electronics*, vol. 65, no. 5, pp. 4331–4337, 2017.
- [11] C. Hu, S. Song, X. Wang, M. Q.-H. Meng, and B. Li, "A novel positioning and orientation system based on three-axis magnetic coils," *IEEE Transactions on Magnetics*, vol. 48, no. 7, pp. 2211–2219, 2012.
- [12] F. H. Raab, "Quasi-static magnetic-field technique for determining position and orientation," *IEEE Transactions on Geoscience and Remote Sensing*, vol. GE-19, no. 4, pp. 235–243, 1981.
- [13] X. Tan, Z. Sun, P. Wang, and Y. Sun, "Environment-aware localization for wireless sensor networks using magnetic induction," Ad Hoc Networks, vol. 98, no. C, 2020.
- [14] M. Hott and P. A. Hoeher, "Underwater communication employing highsensitive magnetic field detectors," *IEEE Access*, vol. 8, pp. 177 385– 177 394, 2020.